JOURNAL OF GEOPHYSICAL RESEARCH, VOL. 105, NO. B3, PAGES 5679-5693, MARCH 10, 2000

Conditions for plumes to penetrate the mantle phase boundaries

Gabriele Marquart and Harro Schmeling
Institute of Meteorology and Geophysics, J.W. Goethe University Frankfurt, Frankfurt/M, Germany

Garrett Ito
School of Ocean and Earth Science and Technology, University of Hawaii at Manoa, Honolulu

Bertram Schott
Department of Geoscience, Uppsala University, Uppsala, Sweden

Abstract. At a depth of ~660 km in the Earth's mantle the spinel-perovskite phase boundary is a prominent barrier for mantle convection. This is due to the negative Clapeyron slope of the phase equilibrium curve which leads to an elevation of the phase boundary within hot upwellings causing negative buoyancy forces. We have investigated the conditions for rising plumes either to penetrate and pass the spinel-perovskite phase boundary or to stick and spread below it by studying the fundamental physics of this process. The plume heads were simply modeled as hot three-dimensional (3-D) spheres or 2-D cylinders. A simple calculation balancing the positive thermal and the negative phase bouyancy forces leads to a better parameterization using two dimensionless quantities. In addition to the phase buoyancy parameter, we defined a deflection parameter, relating the elevation of the phase boundary to the plume head radius to account for the geometrical shape of a plume head. This parameterization is further tested with numerical models that include the effects of thermal diffusion, latent heat, the olivine-spinel phase boundary at a depth of 410 km, and temperature and/or phase-dependent viscosity structure. For laboratory estimates of the slope (-3 MPa/K) and density increase at the spinel-perovskite phase boundary (250 kg/m^3) our models predict that plumes with excess temperatures of 50°-600°C will stick at the top of the lower mantle if their head radii are less than ~100 km. Plumes will penetrate into the upper mantle if plume head radii exceed 100 km. While the style of plume penetration or spreading at the top of the lower mantle strongly depends on the viscosity structure, the conditions for penetration do not. All rising hot volumes with nonpenetrating conditions stick at the top of the lower mantle and spread laterally, independent of their viscosity structure. For weakly nonpenetrating conditions, heat diffusion increases the radius of the hot volume and leads to penetration during a secondary stage. For strongly nonpenetrating conditions, spreading at the top of the lower mantle drives a mechanically coupled counterflow in the upper mantle, which is stable for a very long time. For volumes with an excess temperature of more than 350°C heat diffusion across the phase boundary will eventually inhibit this counterflow and stabilize a thermally coupled flow which might entrain some material of the hot volume. However, our results suggest that the spinel-perovskite phase boundary is unlikely to inhibit the penetration of mantle plumes of the size thought to have generated many flood basalt provinces and hotspot chains.

1. Introduction

It is generally believed that mantle plumes are concentrated upwellings of hot material presumably created at the core-mantle boundary [*Morgan,* 1971]. After detaching from the thermal boundary layer, plumes are thought to rise through the entire mantle, eventually reaching the base of the lithosphere, where partial melting occurs and feeding volcanic chains at the surface. The existence of plumes in the Earth's mantle had only been confirmed in a few cases by seismic tomography [e.g., *VanDecar et al.*, 1995; *Wolfe et al.*, 1997; *Bijwaard and Spakman,* 1999], but the seismic data still do not allow one to clearly distinguish between plume head and tail or even minor internal structures. The dominant driving force of these hot mantle plumes is thermal buoyancy. However, it is well known that at high temperatures and pressures, mantle rocks undergo a number of solid-state phase transitions which change the density and thus the buoyancy. This buoyancy force will be referred to as phase buoyancy in the following.

If we accept a chondritic composition of the original Earth, the fraction of olivine in the Earth's mantle should be ~60-65%.

Paper number 1999JB900413.
0148-0227/00/1999JB900413$09.00

The two major phase transformations of olivine are the olivine-spinel (O-S in the following) and the spinel-perovskite (S-P) transformations. Experimental studies under high pressure and high-temperature conditions in the Mg_2Si0_4-Fe_2Si0_4 system [*Akaogi et al.*, 1989, 1998; *Katsura and Ito*, 1989; *Ito and Takahashi*, 1989] show that for a midmantle temperature of ~1500°C the O-S transformation will occur at a pressure of ~13 GPa while the S-P transformation occurs at a pressure of ~23 GPa. These pressures correspond well with the depths of the 410 and 660 km seismic discontinuities, respectively (see Figure 1).

The presence of these phase transformations and the slopes of their phase equilibrium curves in a P-T diagram have a major influence on the style of mantle convection. While the O-S phase transition curve has a positive slope, releasing heat during the transformation to the high-pressure mineral (exo-thermic phase change), the S-P phase transition curve has a negative slope, consuming heat during the transformation to perovskite (endothermic phase change). As a consequence, rising/sinking material which is hotter/colder than the ambient mantle undergoes the S-P phase transformation at a shallower/deeper level and the O-S transformation at a deeper/shallower level than average. This leads to a vertical deflection of the phase boundaries inside an upwelling or downwelling flow. For a rising hot plume the denser perovskite material at the base of the transition zone results in a negative buoyancy force, and the less dense olivine material at the top of the transition zone results in a positive (phase) buoyancy force. Latent heat associated with these phase changes, however, contributes density variations that partially counteract the buoyancy forces by the phase change [*Schubert and Turcotte*, 1971; *Schubert et al.*, 1975]. But latent heat is only essential in case of low Rayleigh number convection where heat diffusion processes are important. For high Rayleigh number convection the latent heat effect at the phase boundaries can be assumed as adiabatic, and thus a constant temperature jump occurs along the entire phase boundary. Lateral temperature variations within a rising or sinking flow still lead to deflection of the phase boundary and release or consumption of latent heat at elevated or depressed levels and thus may influence the flow. These effects are incorporated in our numerical models, and the overall behavior of plumes is qualified.

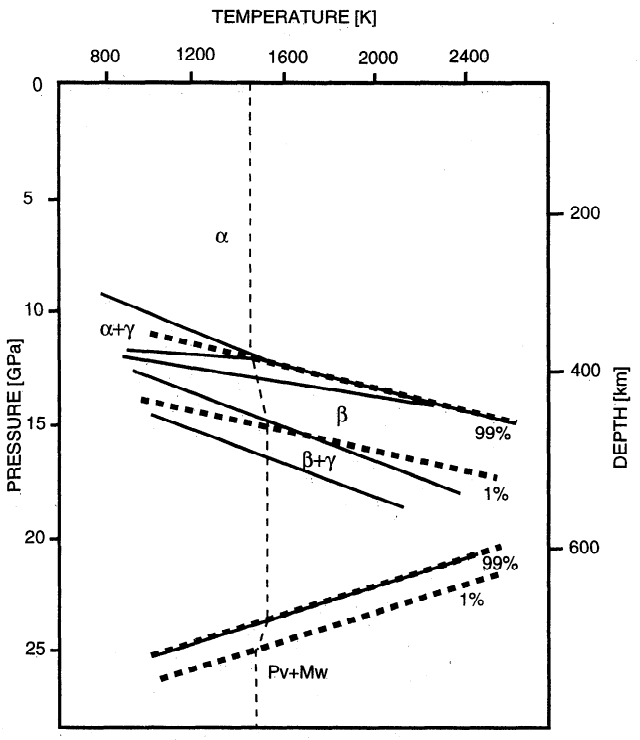

Figure 1. Simplified phase transformation curves of olivine (solid, redrawn after *Akaogi et al.*, [1989]). α, β, and γ indicate the different phases of olivine and Pv+Mw denotes perovskite and muscovite. The transition ranges used for the numerical modeling are indicated by thick dashed curves. The temperature profile used in the numerical modeling is indicated by a thin dashed curves.

A number of recent numerical experiments for whole mantle convection included the S-P phase boundary and studied its effect on the style of convection [*Machetel and Weber*, 1991; *Zhao et al.*, 1992; *Peltier and Solheim*, 1992; *Honda et al.*, 1993; *Tackley et al.*, 1994; *Tackley*, 1995]. They generally found that flow penetration is strongly wavelength dependent, with the longest wavelengths penetrating the S-P phase boundary most easily. They also found that layered convection is more likely for high Rayleigh number convection. This can be explained by the fact that high Rayleigh number convection favors narrow features having more energy at smaller wavelengths [*Tackley*, 1995]. Thus geometry seems to be one of the key parameters to understand penetration or stagnation of flow at the S-P phase boundary.

A few papers specifically dealt with the interaction of a mantle plume with the S-P phase boundary in the Earth's mantle [*Schubert et al.*, 1995; *Nakakuki et al.*, 1994; *van Keken and Gable*, 1995; *Davies*, 1995]. In the first two studies a strongly temperature-dependent viscosity was assumed to investigate the influence of the slope of the Clapeyron curve on the style of mantle convection. As a result they agreed that plume penetration is prevented for a Clapeyron slope more extreme than -3MPa/K. *Nakakuki et al.* [1994] also found a clear relation of plume penetration to the (plume) Rayleigh number, which they interpreted as a dependence of plume penetration on viscosity. *Van Keken and Gable* [1995] modeled a rheological interface at the transition zone separating a less viscous upper mantle from the more viscous mantle beneath. They showed that plumes become strongly narrowed when passing the transition zone and start to show a pulsating behavior. *Davies* [1995] already demonstrated that plumes may penetrate or stagnate at the S-P phase boundary depending on the density increase and the slope of the Clapeyron curve but that, generally, the S-P phase boundary is not a strong hindrance for subducting plates and plumes.

Whether or not a lower mantle plume penetrates into the upper mantle and the amount of mantle mixing that occurs during this process have important implications for large-scale mixing in the Earth's mantle as well as the local-scale chemical heterogeneity of individual hotspots on the surface. While in the work of *Schubert et al.* [1995], *Nakakuki et al.* [1994], *van Keken and Gable* [1995] and *Davies* [1995] the entire convection system in the Earth's mantle was modeled, we focus only on the interaction of a hot rising volume with the S-P phase boundary, which allows us to identify the basic physics. We will show that geometry is an essential parameter and that the reported dependence of plume penetration on Rayleigh number

has to be interpreted as a dependence on the size of the plume head as a characteristic length instead of on the viscosity. We first examine simple analytic descriptions of thermal and phase buoyancy force balance to develop a new parameterization. We then confirm this parameterization with fully dynamic models in two and three dimensions (2-D and 3-D). We find that whether a plume from the lower mantle will penetrate, partially penetrate, or stagnate at the S-P boundary is mainly controlled by the balance of the positive thermal buoyancy force and the negative phase buoyancy force due to the elevation of the S-P boundary above or inside the hot material. The size of the plume or plume head and its excess temperature are the critical geometric and thermal factors that control penetration, partial penetration, or stagnation.

2. A Simplified Model for Plume-Phase Boundary Interaction

Here we assume a first-order phase transformation. The vertical deflection of the phase boundary Δz due to the arrival of a rising or sinking hot or cold volume can easily be estimated from the slope of the phase equilibrium curve

$$b = \frac{dP}{dT} \simeq \frac{\Delta P}{\Delta T}, \tag{1}$$

where P is the pressure, T is the temperature, ΔP is the pressure difference between the deflected and the original phase boundary, and ΔT is the temperature deviation from the average mantle temperature. If we assume that the hydrostatic pressure increases linearly with depth in the Earth's mantle, the deflection is simply given by

$$\Delta z = \frac{b}{\rho_0 g} \Delta T = b_z \Delta T, \tag{2}$$

where ρ_0 is the mantle density, g is the gravity acceleration, and b_z is the slope of the phase equilibrium curve in a depth-temperature diagram.

In this first analysis we do not deal with the problem of plume formation at the core mantle boundary or with the depth dependence of the multiple parameters involved. To keep the problem simple and to focus on the interaction of the plume head with the S-P phase boundary, we have developed a simple model to quantify the conditions for penetrating, partially penetrating, or stagnating plumes. We approximate the plume by a plume head only. This approximation implies that the plume stem is much narrower than the plume head, a reasonable assumption for starting plumes. The plume head is simply approximated by a hot spherical (3-D) or cylindrical (2-D) volume of a given radius r and constant excess temperature ΔT. Such a hot body will stick at the S-P phase boundary if the excess weight of the dense material between the elevated phase boundary and its original level balances the thermal buoyancy of the entire hot volume (Figure 2). Such a volume might not undergo any phase change at all (Figure 2a). This case will be called "no penetration". In the case where the volume starts to penetrate a certain amount and partially undergoes a phase change, it might still stick because the maximum of the negative phase buoyancy is not reached before the center of the volume has risen to $\Delta z/2$ above the original level of the phase boundary (Figure 2b). This case will be called "partial penetration". If the thermal buoyancy is never completely balanced by the negative phase buoyancy, the volume is expected to penetrate. If the slope of the S-P phase equilibrium curve and the corresponding density increase are known, we can use two nondimensional parameters which control the penetration of a plume head of radius r and excess temperature ΔT. The ratio of the thermal to the phase buoyancy is given by

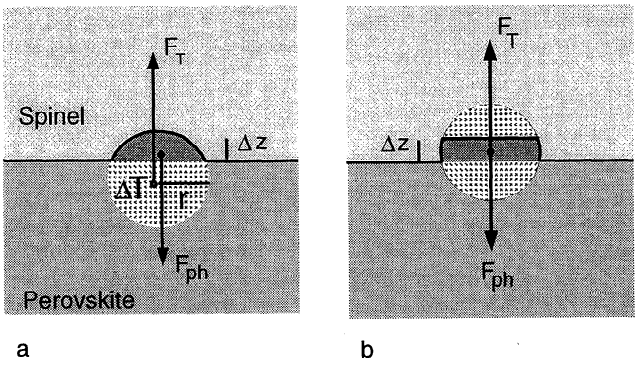

Figure 2. Deflection of the spinel-perovskite phase boundary for a rising hot spherical volume of excess temperature ΔT and radius r. F_T is the positive thermal buoyancy, and F_{ph} is the negative phase buoyancy due to the higher density of perovskite at spinel level. Parameter Δz is the deflection of the phase boundary as defined by the slope of the phase equilibrium curve (equation (2)). (a) Force balance at the phase boundary without any phase transformation (solid curves in Figure 3). (b) Volumes which undergo the maximum possible phase transformation but are still in force balance (dashed curves in Figure 3).

$$P = \frac{\alpha \Delta T \rho_o}{\Delta \rho_{S\text{-}P}}, \tag{3}$$

and the ratio of the elevation of the phase boundary due to the excess temperature ΔT to the plume radius is given by

$$D = \frac{|\Delta z|}{r} = \frac{|b_z| \Delta T}{r}. \tag{4}$$

We call D the deflection parameter. A phase buoyancy parameter P^* was already introduced by *Schubert and Turcotte* [1971] and *Christensen and Yuen* [1985] which together with the Rayleigh number describes the dynamics of a convecting system (e.g., layered versus whole mantle convection). In our notation this parameter P^* is defined as

$$P^* = \frac{\Delta \rho_{S\text{-}P}}{\rho_0 \alpha} \frac{|b_z|}{l} = P^{-1} D, \tag{5}$$

where l is a characteristic length that we define as r but *Christensen and Yuen* [1985] defined as the thickness of the convecting layer. In the case of well-established plume stems or sheets of vertical extent l the parameter P^* is sufficient to describe the force balance at the phase boundary. *Bercovici et al.* [1993] investigated flat sheets of cold slab material resting on the S-P boundary and defined l as the thickness of this sheet. Note that the force balance is independent of ΔT for configurations as stems or sheets. In case of a spherical or flattened rising plume head of radius r (which might be independent of the thickness of the convecting layer and could in principal become as small as Δz) we need two parameters to describe the conditions of penetration and partial penetration accounting for the different geometries of the volumes in which thermal buoy-

ancy and phase buoyancy are created. In the following we used the parameters P^* and D to study the interaction of a rising plume with the S-P phase boundary.

To derive the conditions for penetration or partial penetration as illustrated in Figures 2a and 2b, we calculate the volumes of the elevated perovskite phase for spherical and cylindrical volumes. Equating the corresponding thermal and phase buoyancy forces yields critical curves in the P^*-D space separating regions of penetration, partial penetration and no penetration (Figure 3). Since a rising hotvolume flattens when it experiences the S-P phase transition, we also calculate the corresponding curves for ellipsoids and elliptically flattened cylinders with the flattening parameter f ($f = (a-b)/a$, where a and b define the half-axis of the ellipsoid) indicated (see appendix). Flattening will generally enhance the effect of negative phase buoyancy and impede penetration because flattening increases the volume proportion between 660 km and the deflected phase boundary.

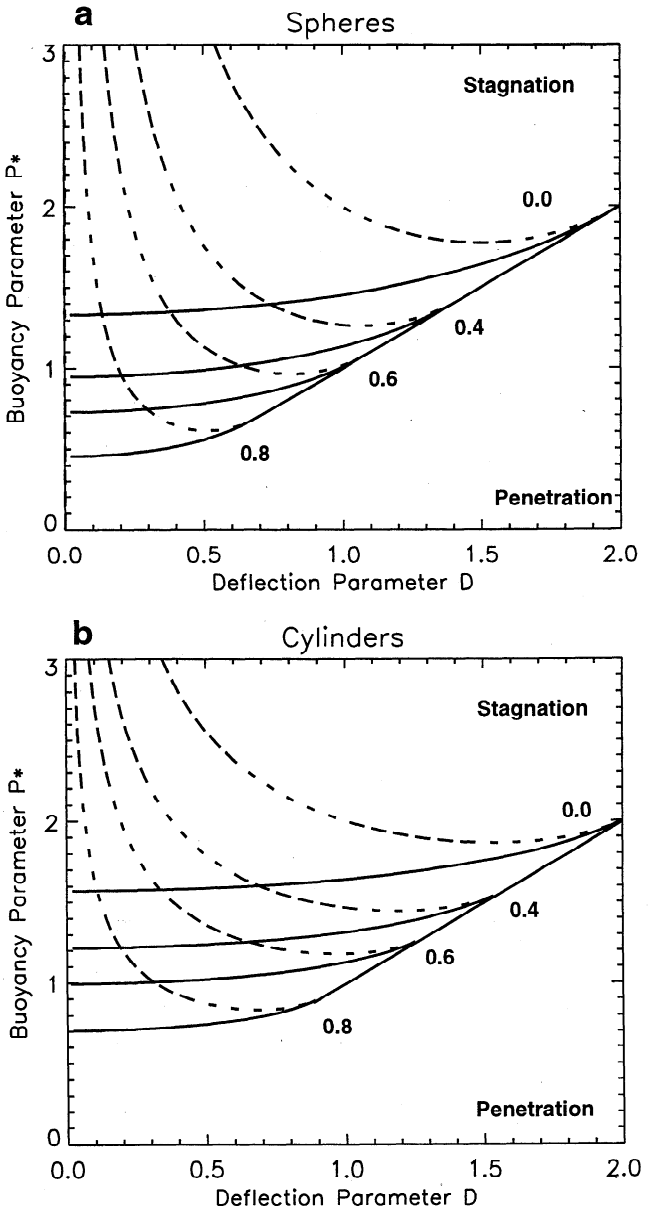

Figure 3. Conditions for hot (a) spheres or (b) cylinders to penetrate or stagnate at the S-P phase boundary depending on the parameters P^* and D (as defined in equations (4) and (5)). Dashed curves indicate volumes where thermal and phase buoyancy are balanced without any phase change at all (Figure 3a); solid curves indicate volumes with maximum possible phase transformation but still balance between thermal and phase buoyancy (Figure 3b). The curves are given for different flattening parameters 0.0, 0.4, 0.6, and 0.8.

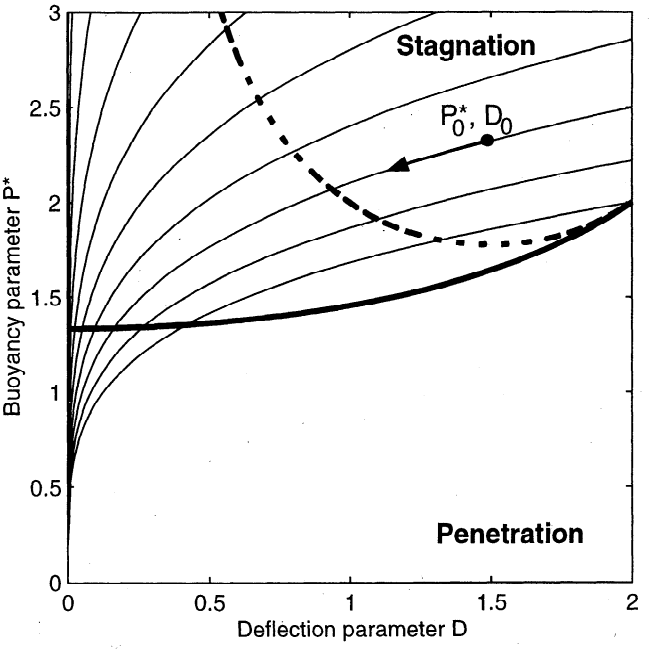

Figure 4. P^*,D paths for spherical volumes undergoing heat diffusion. A volume with the initial values P^*_0, D_0 changes its excess temperature and radius by heat diffusion which leads to a change in P^* and D parameters along the path as indicated by the arrow.

The solid curves in Figure 3 indicate hot volumes that do not undergo any phase change at all (compare Figure 2a) while the dashed curves indicate the case in which a maximum of the plume volume has changed phase but there is still force balance between thermal and phase buoyancy (Figure 2b). In this simple approach all "plume" volumes with P^* and D values above the dashed curves in Figure 3 will stick, those below the solid curves will penetrate, and those between the dashed and solid curves are expected to partially penetrate. It is clear that all volumes with $P^* < D$ (or $P > 1$) will penetrate. If $D > 2$, the deflection of the phase equilibrium curve would be greater than the diameter of the volume. In this case any plume head with $P > 1$ would detach from the S-P boundary and continue to rise in the perovskite state for some distance.

These simple relations do not include the effect of heat diffusion. However, we may estimate this effect by assuming that the heat content of the hot volume may diffuse during ascent, leading to an increase in sphere or cylinder radius and a decrease of excess temperature. The P^* and D values of a volume starting with an initial ΔT and r (P^*_0,D_0) are shifted along paths indicated on Figure 4 with a rate roughly halving P every 0.2 diffusion times t_{diff} ($= r^2/\kappa$, where κ is the thermal diffusivity). Finally, all paths enter the partial penetration and the penetration regime. This behavior, however, would only be important if the geometrical shape would be preserved and the diffusion time would be smaller or of the same order as the Stokes Sphere rising time ("Stokes time")

$$t_{Stokes} = \frac{\mu}{r\ g\ \rho_0\ \alpha\ \Delta T}, \quad (6)$$

which is defined as the time a hot Stokes sphere rises ⅓ of its radius, where μ is the viscosity of the surrounding medium. For hot volumes in the penetration field the geometrical shape during the phase transition can be assumed to be largely preserved, but the diffusion time is much larger than the Stokes time, and thus diffusion is unimportant. Volumes in the stagnation field stick at the phase boundary, and diffusion might become important. However, they also become more oblate by lateral spreading and change their shape considerably, and only parts of the initial volume might penetrate in a final stage. We can also define a sphere Rayleigh number based on the radius of the sphere, $Ra_{sp} = t_{diff}/t_{Stokes}$, which controls the relative importance of thermal diffusion. With this definition, the thin lines in Figure 4 represent lines of constant Ra_{sp}. In general, spheres with small D and large P^* are associated with small Ra_{sp}: thus diffusion is important only for P^*-D paths in the upper left corner of Figure 4.

When considering the Earth, it is of interest to show explicitly the excess temperature and radii of plumes in the different regimes of penetration and stagnation. For the density change and the slope of the phase equilibrium curve according to Table 1 we have calculated the P^* and D values depending on r and ΔT. The diagram is given in Figure 5 for spheres. For a realistic range of plume excess temperatures (<400°C), spherical volumes with radii smaller than ~130 km will stick or only partially penetrate the S-P phase boundary. Figure 5 also indicates that for realistic Earth's parameters "penetration" depends on P^* alone, while for "partial penetration" P^* and D are needed.

3. Numerical Model

While the simple force balance approach in section 2 is already quite instructive and shows the principal behavior of rising hot volumes at the S-P phase boundary, the entire interaction is much more complicated. Important effects may include heat diffusion, deformation of the plume at the phase boundary, latent heat, the O-S phase boundary, and rheology. We have therefore carried out a series of 2-D and 3-D numerical experiments for rising hot volumes.

Table 1. Parameters and Their Numerical Values Used in This Study

Parameter	Symbol	Numerical Value
Reference mantle density	ρ_0	4250 kg/m^3
Density jump at O-S phase boundary	$\Delta\rho_{O\text{-}S}$	196.3 kg/m^3
Latent heat at O-S phase boundary	$H_{O\text{-}S}$	60.3 x 10^3 J/kg
Slope of O-S phase equilibrium curve with respect to depth	$b_{zO\text{-}S}$	68.4 m/°C
Density jump at S-P phase boundary	$\Delta\rho_{S\text{-}P}$	250.3 kg/m^3
Latent heat at S-P phase boundary	$H_{S\text{-}P}$	-65.5 x 10^3 J/kg
Slope of S-P phase equilibrium curve with respect to depth	$b_{zS\text{-}P}$	-74.6 m/°C
Thickness of model box	h	.5 10^6 m
Thermal expansivity	α	2.5 x 10^{-5} K^{-1}
Thermal diffusivity	κ	10^{-6} m^2/s
Gravity acceleration	g	9.85 m/s^2
"Plume" excess temperature	ΔT	50°-1500°C
Specific heat (at constant pressure)	c_p	1.3 x 10^{3}J/kgK
Scaling viscosity	μ	10^{21} Pa s

Notice that we assumed 65% of olivine in the mantle to estimate the numerical values of the density jumps and the latent heats.

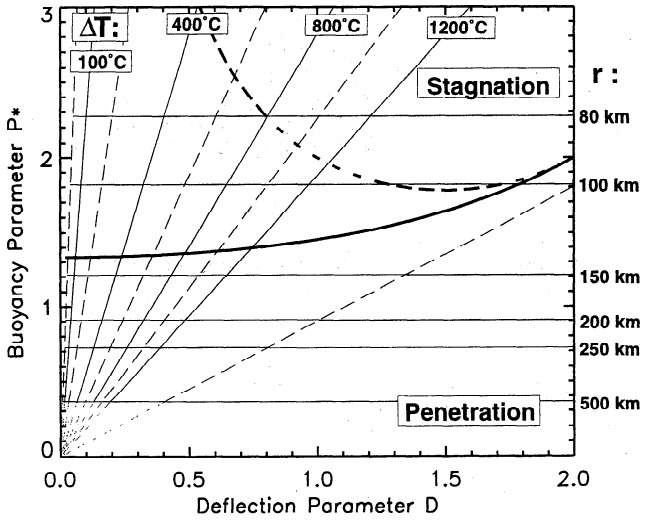

Figure 5. Lines of constant excess temperature ΔT and radius r in a P^*,D diagram for spherical volumes. The values for the various parameters to calculate P^* and D are given in Table 1. Note that r is valid for hot volumes with constant excess temperature; to compare to plumes with a temperature gradient inside the plume head, one has to multiply r by a factor of ~1.43.

3.1. Numerical Implementation of Phase Boundaries

We approximated the phase transitions occurring in the mantle transition zone by simple linear phase equilibrium curves that define two ranges for the transition of olivine to spinel and spinel to perovskite. In each range the fraction of transformed material increases linearly with depth. Figure 1 shows the ranges for 1%-99% transformation plotted onto the phase diagram. The phase transformations are estimated by linear functions as

$$T_{O\text{-}S,\ S\text{-}P} = \frac{1}{b_{z_{O\text{-}S,\ S\text{-}P}}}\ z - T^*[°C], \quad (7)$$

where T^* is the projected intercept temperature of the respective phase equilibrium curve at zero depth (for 1% spinel, -4500°C; for 99% spinel, -5700°C; for 1% perovskite, 9888°C; and for 99% perovskite, 10199°C). The O-S transformation as modeled here combines a series of phase changes (α to β to γ phase).

Seismological findings and experimental evidence [*Ito and Takahashi*, 1989] indicate that the S-P phase change is very sharp, occurring over a narrow pressure interval. Numerical limitations, however, required us to define a range of ~50 km, or three numerical grid points. While this width is broader than that anticipated in the Earth, the effect of this width on convection is likely to be important only when the width is comparable to convective features [*Tackley*, 1995].

The density changes associated with both phase changes were estimated from laboratory data. For O-S we used the work of *Akaogi et al.* [1989, Table 4] to estimate the density change to be 302 kg/m^3 and for S-P we used a value of 385 kg/m^3, in agreement with *Chopelas and Boehler* [1989]. The effective density change was estimated by assuming 65% olivine in the Earth's mantle. For further values see Table 1.

3.2. Method

In the numerical calculations the equations of conservation of mass, momentum, and energy were solved in 2-D and 3-D Cartesian and axisymmetric spherical shell geometry. We assumed

an incompressible fluid and applied the Boussinesq approximation: that is, the density variations with temperature and phase are only considered in the buoyancy term but additionally accounted for latent heat at the phase transitions.

The effect of latent heat was considered in the energy conservation equation where we took into account the "convective derivative". This includes the change of the position of the phase boundaries with time and due to advection. We also took into account the effect of a spatial variation of viscosity due to temperature, depth, and mineral phase. Thus the equations in nondimensional variables become

$$0 = \nabla p + \mu\nabla^2\vec{v} + 2(\nabla\mu\nabla)\vec{v} - \nabla\mu\times(\nabla\times\vec{v}) - (Ra\ T - Ra_c\ \Delta\rho_{O\text{-}S}\ f_{O\text{-}S}\ \ Ra_c\ \Delta\rho_{S\text{-}P}\ f_{S\text{-}P})\vec{e}_z\ , \quad (8)$$

$$-\frac{\partial T}{\partial t} = -\nabla^2 T + \vec{v}\,\nabla\,T + H_{O\text{-}S}\left(\frac{\partial f_{O\text{-}S}}{\partial t} + \vec{v}\,\nabla f_{O\text{-}S}\right) + H_{S\text{-}P}\left(\frac{\partial f_{S\text{-}P}}{\partial t} + \vec{v}\,\nabla f_{S\text{-}P}\right), \quad (9)$$

$$\nabla\,\vec{v} = 0\ , \quad (10)$$

where p is the flow pressure, μ is the viscosity, v is the flow velocity, t is time; $\Delta\rho_{O\text{-}S}$ and $\Delta\rho_{S\text{-}P}$ are the density jumps associated with the phase transformation, $f_{O\text{-}S}$ and $f_{S\text{-}P}$ are the phase functions that define the percentage of transformed material in the phase transition range, and $H_{O\text{-}S}$ and $H_{S\text{-}P}$ are the amounts of latent heat.

$$Ra = \frac{\rho_0\, g\, \alpha\, \Delta T\, h^3}{\kappa\, \mu_0} \quad (11)$$

is the Rayleigh number and

$$Ra_c = \frac{\rho_0\, g\, h^3}{\kappa\, \mu_0} \quad (12)$$

is the phase buoyancy (or chemical) Rayleigh number which appear owing to the non dimensionalization of (8)-(10). The definitions and numerical values of the various parameters are given in Table 1.

Temperature and depth-dependent viscosity were simply modeled by

$$\mu = \exp(-c_1\ T + c_2\ z)\ , \quad (13)$$

where c_1 and c_2 are constants which had been adjusted to model a viscosity of ~10^{21} Pa s at the S-P transformation depth and an additional increase of 1 order of magnitude down to the bottom of the model. The reduction of the viscosity with temperature was 1 order of magnitude for 500°C (which is in agreement with an activation energy of ~150 KJ mol^{-1}). For phase-dependent viscosity we assumed an increase in viscosity from the upper to the lower mantle by a factor of 30, and we used the phase function $f_{S\text{-}P}$ to calculate the spatial variation in viscosity.

Equations (8)-(10) represent a system of five partial differential equations, from which we solved for the three components of the flow velocity, the dynamic pressure, and the temperature. For flow solutions in Cartesian geometry we applied a spectral approach, solving for Fourier modes in horizontal directions, and we applied a finite difference scheme in vertical directions. For the axisymmetric geometry we used finite differences in both directions. The nonlinearity in the force equilibrium equation (equation (9)) due to lateral variations in viscosity (caused by temperature-dependent or phase-dependent viscosity, only considered for the Cartesian geometry cases) was taken into consideration by splitting the viscosity into constant and depth-dependent parts and higher-order variations. Treating these higher-order modes as an additional load vector, the force balance equation was solved iteratively with a wavenumber-dependent damping term. We solved the energy equation using an explicit time stepping with dynamic time step control and local upwind differencing for the convective derivatives. The time derivatives of the phase functions $f_{O\text{-}S}$ and $f_{S\text{-}P}$ were considered by a backward stepping in time.

3.3. Model Layout

We calculated models with a constant viscosity of 10^{21} Pa s, a phase-dependent viscosity with 10^{21} Pa s for the olivine and spinel phase and 3×10^{22} Pa s for the perovskite phase, where the viscosity was linearly dependent on the amount of perovskite in the transition regime, and a temperature and depth-dependent viscosity as described in section 3.2.

The mechanical boundary conditions do not play a significant role nor does the size of the numerical box. We used periodic sidewalls and no slip at the lower and free slip at the upper boundary. The size of the numerical box was 3000 km in the horizontal and 1500 km in the vertical. We solved for 128 horizontal nodes (64 spectral modes) and 80 vertical nodes in the Cartesian models and 80 x 80 to 160 x 160 nodes for the axisymmetric models. We restricted the model to the upper 1500 km of the mantle since we are primarily interested in the interaction of a rising volume with the phase boundaries and not in the formation of plumes at the core-mantle boundary.

Starting temperature conditions included temperature jumps of 50.3°C and -54.6°C across the O-S and S-P phase transitions, respectively (Figure 6b). We used a background temperature of 1480°C and added the respective temperature variations across the phase transformation ranges according to the amount of transformed material. This initial temperature distribution was designed to approximate the temperature structure within the transition zone of a vigorously convecting mantle.

We ran a large number of 2-D Cartesian models for rising horizontal cylinders and a few fully 3-D Cartesian and axisymmetric spherical shell models for rising spheres. An initially circular (cylindrical or spherical) temperature anomaly was centered at a depth of ~400 km below the S-P phase boundary. The excess temperature was a maximum of ΔT_{max} at the center and decreased as a cosine function to the ambient temperature at a radius of r. To compare the numerical models to the analytical results, we examined ΔT_{max} values between 50°C and 2500°C and r values between 114 and 494 km. A sketch of the model geometry and boundary conditions is given in Figure 6.

For the numerical models we had to define an effective radius r_{eff} according to that which yielded the same total thermal buoyancy force as a volume with a uniform temperature anomaly $\Delta T = \Delta T_{max}$ (as done in the analytic models). For cylinders $r_{eff} = 0.6802r$, and for spheres $r_{eff} = 0.7126r$. Using these excess temperatures and effective radii we have examined models with D values <2 and P^* values <3. In all cases the sizes of the rising volumes are considerably larger than the width of the S-P phase transition.

A characteristic timescale that we used to characterize the strength of penetration through the phase boundaries is the Stokes time (equation (6)). For our parameters the Stokes times range from ~0.2 to 15 Myr, with larger values associated with small volumes. Figure 7 shows the Stokes time depending on excess temperature and effective radius for a constant viscosity of 10^{21} Pa s. A rising volume was defined as penetrating when it passes the S-P phase boundary in <15 times its Stokes time. Volumes that showed considerable lateral spreading at the S-P phase boundary but penetrated at a time >15 Stokes times are

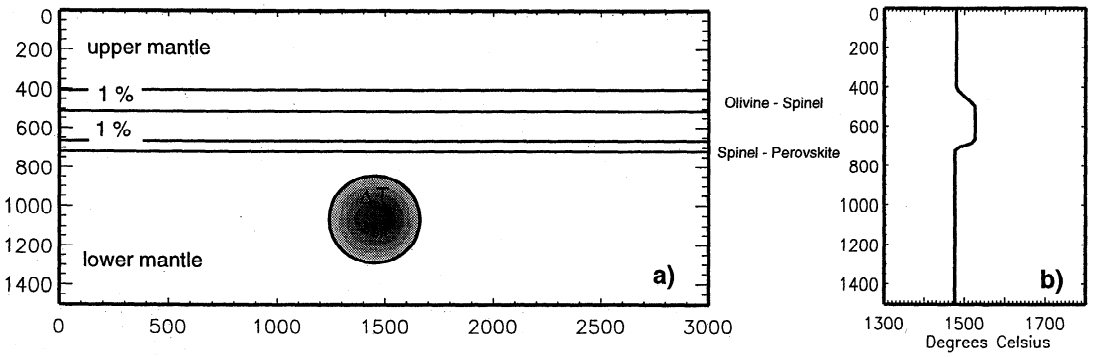

Figure 6. (a) Sketch of the model layout for the numerical modeling. (b) Initial temperature profile.

classified as "delayed penetration". Volumes that failed to penetrate the S-P phase boundary and caused mechanically coupled counterflow in the upper mantle by lateral spreading are defined as "stagnating".

3.4. Model Results

Figure 8 shows the results of the numerical models together with analytic curves with flattening parameters that best fit the numerical results. In general, the behavior of the hot volumes in the numerical models is well described by the simple analytical approach. It also demonstrates that for volumes in the partial penetration regime the P* parameter alone is not sufficient to decide about penetration or stagnation. For excess temperatures of more than ~1200°C the numerical models deviate from the analytical behavior (Figure 8) in that they have a stronger penetration ability. This result reflects the cosine taper in the initial temperature which allows at least the outer edges of the plume to penetrate the S-P phase boundary and rise to the O-S phase boundary, upon which buoyancy is enhanced. For ΔT_{max}> ~1200°C these effects enhance penetrability whereas for ΔT_{max} < ~1200°C these effects are unimportant. Realistic plume temperature excesses in the Earth are <1200°C and therefore the O-S boundary is likely to be unimportant for the question of plume penetration or stagnation.

Flattening is an important parameter for volumes with *P*-D* parameters close to the transition from penetration to stagnation. The best-fitting analytical *P*-D* curves are those with a flattening parameter of 0.4 for cylinders and 0.3-0.2 for spheres (but the value for spheres is not well confined). For spheres the transition between stagnation and penetration seems to be sharper than for cylinders. This might be due to the circular flattening of spherical volumes, which causes a faster increase in volume with negative phase buoyancy below the phase boundary.

Even though very different viscosity cases were examined (constant viscosity, viscosity change at the S-P transition of a factor of 30, and depth- and temperature-dependent viscosity) we found the penetration or stagnation of the rising hot volumes to be essentially insensitive to the viscosity specified. Volumes with *P** and *D* values between the two analytical curves (this regime corresponds to the partial penetration regime in the analytical approach) initially stick at the S-P phase boundary, but after some time of heat diffusion they grow enough to rise as a whole, carrying lower mantle material upward. During the diffusion stage, upper mantle material is warmed up and may well be entrained in the plume as it continues to rise through the upper mantle.

To illustrate the process of penetration or stagnation in more detail we will discuss a few 2-D examples (Figures 9-13) for which the principal interaction with the mantle phase boundaries is easier to visualize than for the 3-D models. Essentially, the 2-D and 3-D cases show the same behavior.

3.4.1. Penetration case. We first consider a large hot volume with *P-D* parameters in the penetration field of Figure 3. We used the values from Table 1, ΔT = 400°C, and r_{eff} = 153 km. This is equivalent to *P** = 1.147 and *D* = 0.195. In a constant viscosity medium the volume penetrates rapidly, largely unaffected by the phase boundaries, and a large plume head develops in the upper mantle (Figure 9a, left). The phase boundary reduces the rise velocity, but the volume passes the S-P phase boundary on a timescale of ~6 Myr, or ~12 Stokes times. The amount of lateral spreading before final penetration is very small. The maximum rise velocity of 14 cm/yr occurs when the hot volume rises through the upper mantle due to the additional buoyancy of the O-S phase boundary, while the rise velocity is only ~3 cm/yr when the volume is passing through the S-P phase transition (Figure 9c). The streamlines in Figure 9a (shown on right) show a style of whole mantle convection.

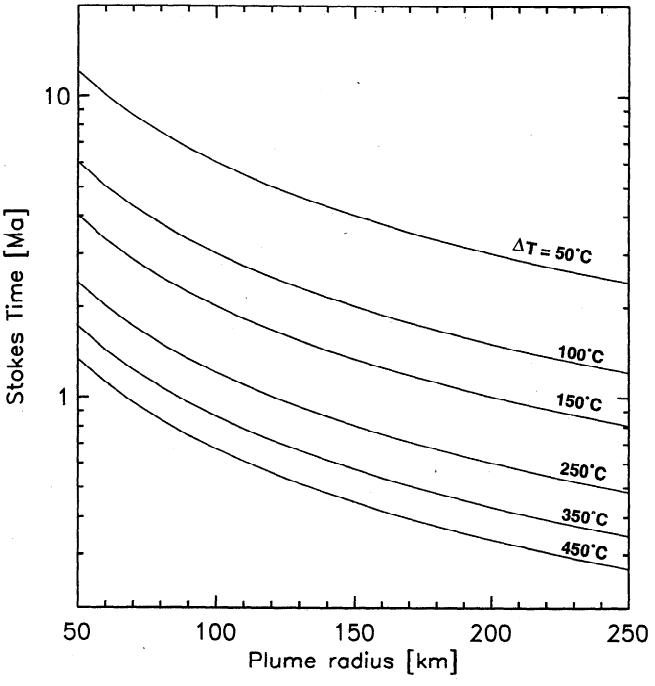

Figure 7. Characteristic rising times (Stokes time) for spherical volumes depending on excess temperature and radius (and the parameters from Table 1).

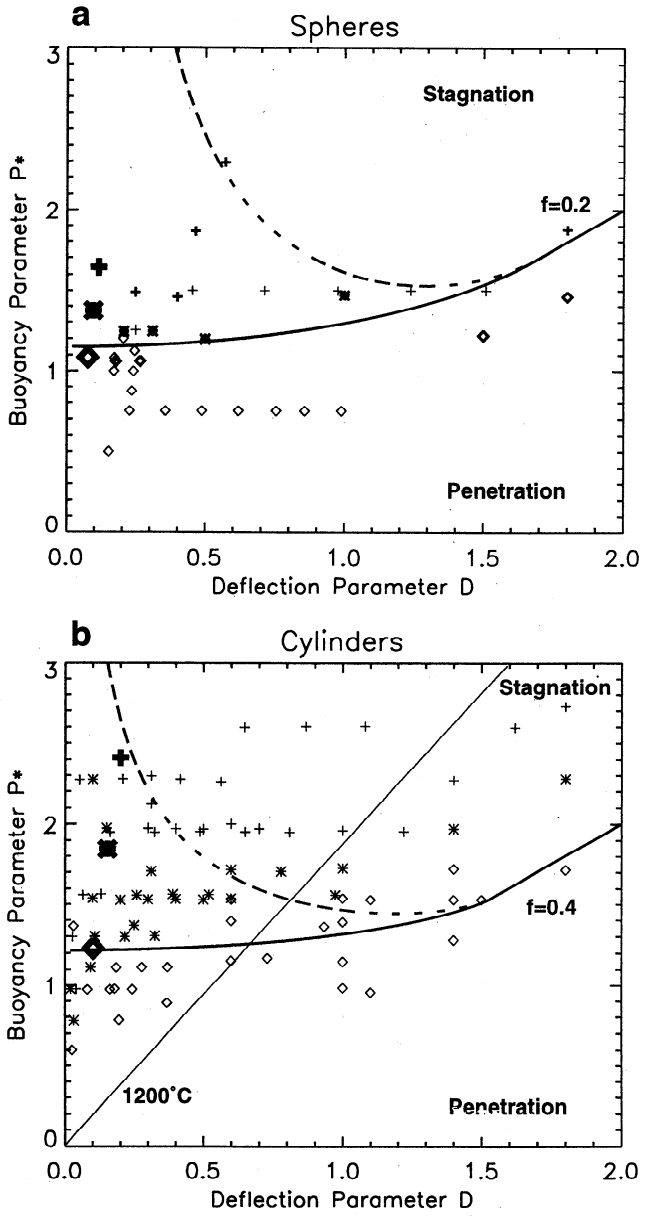

Figure 8. Results of the numerical models together with analytical curves for a flattening parameter of 0.4 for cylinders and 0.2 for spheres. Diamonds: The hot volume passed the S-P phase boundary in less than 10 Stokes times. Stars: The hot volume sticks at the S-P phase boundary and spreads laterally but passed through as a whole in more than 15 Stokes times. Crosses: The hot volume sticks at the S-P phase boundary and spreads laterally, starting mechanically coupled counterflow in the upper mantle. (a) Results for spheres. Thin symbols are results obtained with the axisymmetric shell code; thick symbols are obtained with the fully 3-D Cartesian code. (b) Results for cylinders (2-D Cartesian model). The P^*, D curve corresponding to a volume with an excess temperature of 1200°C is shown by a straight line. Large symbols are approximated values for models by *Nakakuki et al.* [1994] in 2-D and by *Davies* [1995] in 3-D (axisymmetric code).

If a large viscosity change of a factor of 30 occurs across the S-P phase boundary (see Figure 10c, far right), the hot volume will penetrate into the upper mantle by establishing a narrow tube with an initially small plume head in the upper mantle (Figure 10a). This behavior is caused by the high viscosity of the material in the perovskite state which inhibits material supply to the upper mantle. Spreading at the S-P phase boundary is a slow process as is the material transport from the lower to the upper mantle. A broad upwarping of the S-P phase boundary is maintained for a long time (here more than 150 Myr). Convective flow is much more vigorous in the less viscous upper mantle compared to the lower mantle but the streamlines (Figure10 a) go through the entire model box establishing a large-scale circulation with a considerable amount of mass exchange across the phase boundary. The Stokes time based on the lower mantle viscosity is 15 Myr.

A model with temperature- and depth-dependent viscosity is shown in Figure 11. In general, this model is similar to the constant viscosity case. However, vertical flow is more concentrated within the central low viscosity region, and no spreading at the S-P boundary is observed. The reduced viscosity in the hot central part together with the positive buoyancy at the O-S phase boundary also leads to a confinement of the flow, which in some other models even resulted in the detachment of small blobs. The Stokes time based on the viscosity of the mantle at 600 km depth is 0.9 Myr. Thus for the variable viscosity cases penetration is also completed after ~12 Stokes times.

3.4.2. Delayed penetration case. A model in the transition range between penetration and stagnation is shown in Figure 12 for the case of temperature- and depth-dependent viscosity. This model was calculated for $P^* = 1.72$ and $D = 0.31$, which is equivalent to an effective radius of 106 km and an excess temperature of 425°C using the scaled numbers of Table 1. This model shows considerable spreading below the S-P phase boundary (at time 35 Myr) with a weak counterflow in the upper mantle, which is clearly indicated on the horizontal flow profile in Figure 12c. The root-mean-square velocity plot shows that the volume sticks at the S-P phase transition for ~20-30 Myr, or 18-27 Stokes times. The partial penetration regime is broader for cylinders than for spheres (Figure 8). This is due to the fact that the circular spreading of a sphere increases the amount of material deflecting the phase boundary upwards more effectively and inhibits penetration.

3.4.3. Stagnation case. A hot volume that does not rise into the upper mantle but stagnates at the phase boundary is shown in Figure 13 (with the values $P^* = 2.28$ and $D = 0.41$, which corresponds to an effective radius of 79.3 km and an excess temperature of 425°C). For stagnation cases the differences between the three viscosity cases are small. Here we show again only the case for variable viscosity. The rising volume sticks and spreads at the base of the transition zone, initiating layered convection in the upper mantle by mechanical coupling. Subsequently, heat is lost mainly by conduction. After some time the lateral spreading weakens, and thermal coupling across the S-P phase boundary takes over. For very late times this may lead to some upwelling of plume material into the upper mantle. This upwelling occurs at ~200 Ma or ~130 Stokes times.

The initial temperature field assumed temperature jumps in the transition zones according to the amount of latent heat release or consumption, implying vigorous convection flow across the phase boundaries. This might not be in accordance with stagnating plumes. In the case of a constant background temperature the deflection of the S-P phase boundary is somewhat larger. This implies that plume penetration is impeded, but if penetration has started, it is more effective because of additional thermal buoyancy. By carrying out a few models with constant temperature background we found, however, that the differences are generally very small and have no influence on the overall interpretation.

4. Discussion and Conclusion

We have investigated the conditions for rising hot material in the Earth's mantle to pass the S-P phase boundary and to pene-

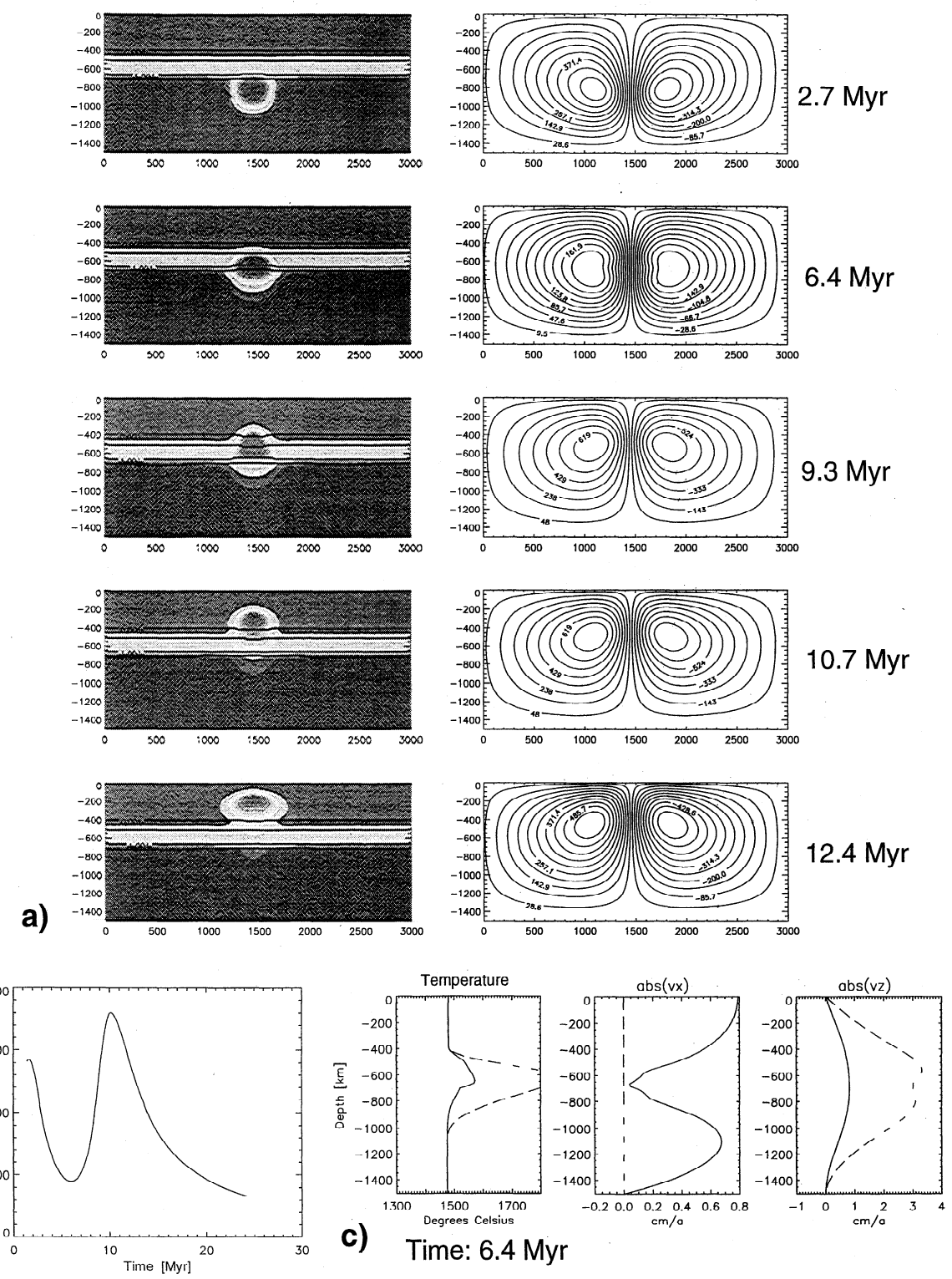

Figure 9. Penetrating hot volume in an isoviscous mantle for parameters $P^* = 1.147$, $D = 0.195$. (a) Temperature field (shown at left) and flow pattern (shown at right) for successive stages of a rising volume. The thick horizontal lines on the temperature field show the 1% and 99% levels for the O-S and S-P phase boundaries.(b) Root-mean-square velocity as a function of time. (c) Depth profiles for temperature and horizontal and vertical flow averaged for the whole model (solid curves) and along a central line through the hot volume (dashed curves) for a typical stage for the interaction with the S-P phase boundary. Stokes time for this calculation is 0.5 Myr.

trate into the upper mantle. Our analytic description predicts that the conditions for a hot volume to pass the S-P phase boundary can be described by two dimensionless parameters, P^* and D, where P^* is the phase buoyancy parameter and D is a characteristic geometric parameter giving the relation between the upward deflection of the S-P phase boundary and the radius of the volume. Numerical models are in agreement with the analytical model, but show that flattening has to be taken into account. For

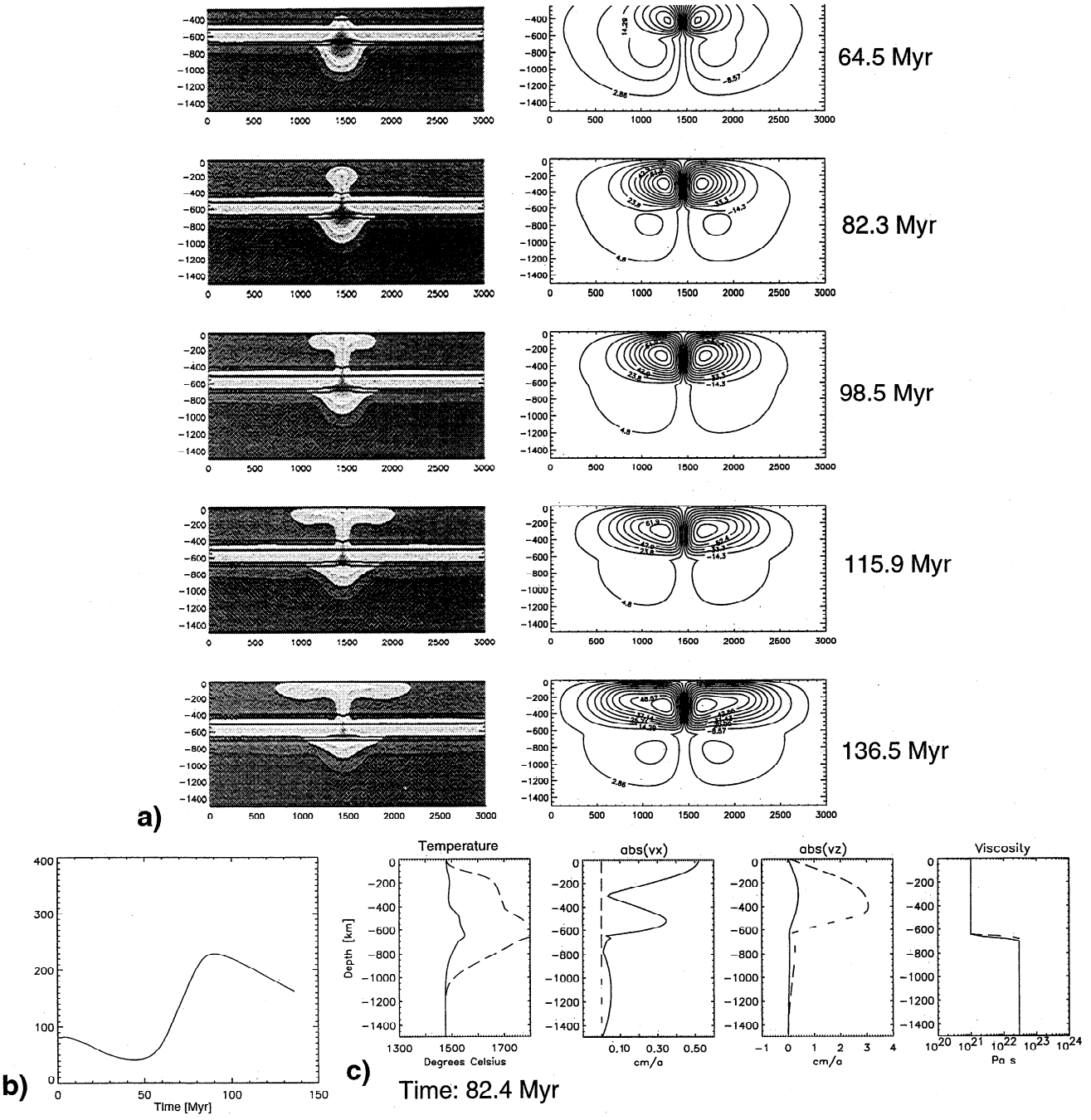

Figure 10. As in Figure 9, but for phase-dependent viscosity with a viscosity jump of a factor of 30 across the S-P phase boundary. See also viscosity profiles in Figure 10c. Stokes time based on lower mantle viscosity is 15 Myr.

a flattening of 0.2-0.4 we obtained the best fit between analytic model and numerical results. Depending on the P^* and D values, we can define three different regimes for the interaction of a hot volume with the S-P phase boundary:

1. In the penetration regime the thermal buoyancy exceeds negative phase buoyancy, and the volume passed the S-P phase boundary in <15 Stokes times. No mixing occurs with the adjacent mantle material during the penetration. The shape of the volume is largely preserved for constant viscosity, and the style of convection is whole mantle flow. Phase- and temperature-dependent viscosity results in a narrowing of the flow when passing the S-P phase boundary. This behavior has already been reported by *van Keken and Gable* [1995], who found the thinning to be strongly dependent on the viscosity contrast but less pronounced in 3-D compared to 2-D. In scaled numbers and for mantle conditions all volumes with effective radii of more than ~130 km will lie in this regime.

2. In the partial (or delayed) penetration regime the phase buoyancy exceeds thermal buoyancy, but parts of the hot volume undergo phase transformation. The volume sticks at the S-P phase boundary and starts to spread. Thermal diffusion increases the radius, and the volume passes the S-P phase boundary in more than 15 Stokes times. Because of the thermal growth of the volume at the S-P boundary some upper mantle material will

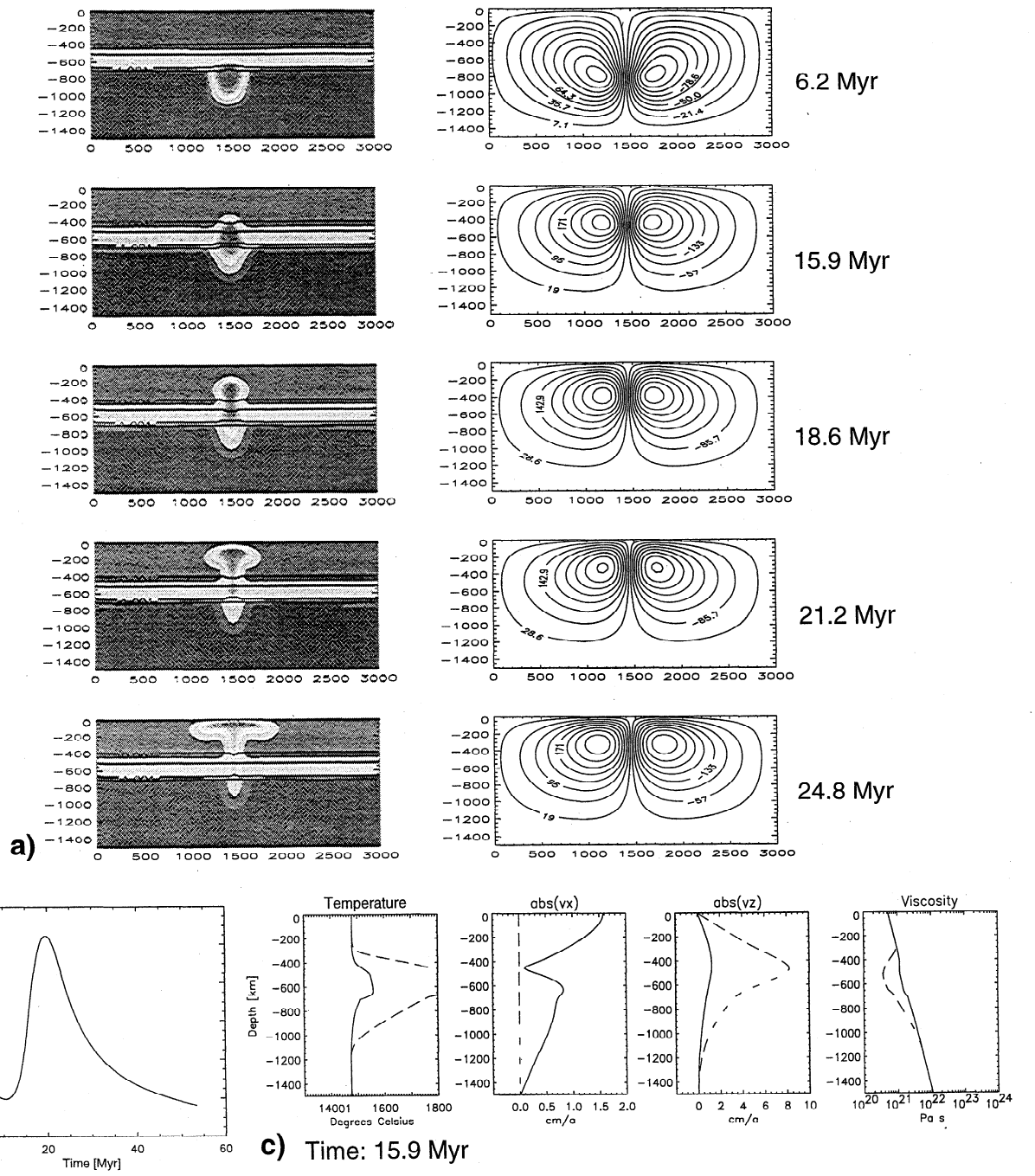

Figure 11. As in Figure 9, but for temperature- and depth-dependent viscosity. See also viscosity profiles in Figure 11c. Stokes time based on the viscosity of the surrounding mantle at 600 km depth is 0.8 Myr.

become entrained. Volumes with effective radii between 90 and 130 km and excess temperature between 50° and 200°C are in this regime. For hotter volumes the phase buoyancy effect becomes more pronounced: therefore a hot plume with small effective radius (<100 km) already lies in the stagnation regime.

3. In the stagnation regime the phase buoyancy exceeds thermal buoyancy, and no phase transformation occurs: the volume is entirely below the elevated phase boundary. Lateral spreading below the phase boundary is maintained for a long time, leading to mechanically coupled flow in the upper and lower mantle. When the volume has flattened and the driving force for the mechanically coupled flow has vanished, thermal diffusion across the phase boundary may lead to an upwelling flow with some degree of mixing between plume and mantle material. Volumes with radii <~80 km and excess temperature <400°C are in this regime. However, even for volumes in the nonpenetration region, thermal diffusion across the S-P phase transition might lead to a central upwelling in the upper mantle after very long times.

Using different viscosity structures we found that the style of penetration of a hot volume into the upper mantle strongly depends on the viscosity structure but not the conditions for penetration. This finding seems to contradict earlier results on plume penetration by *Nakakuki et al.* [1994], who studied plumes

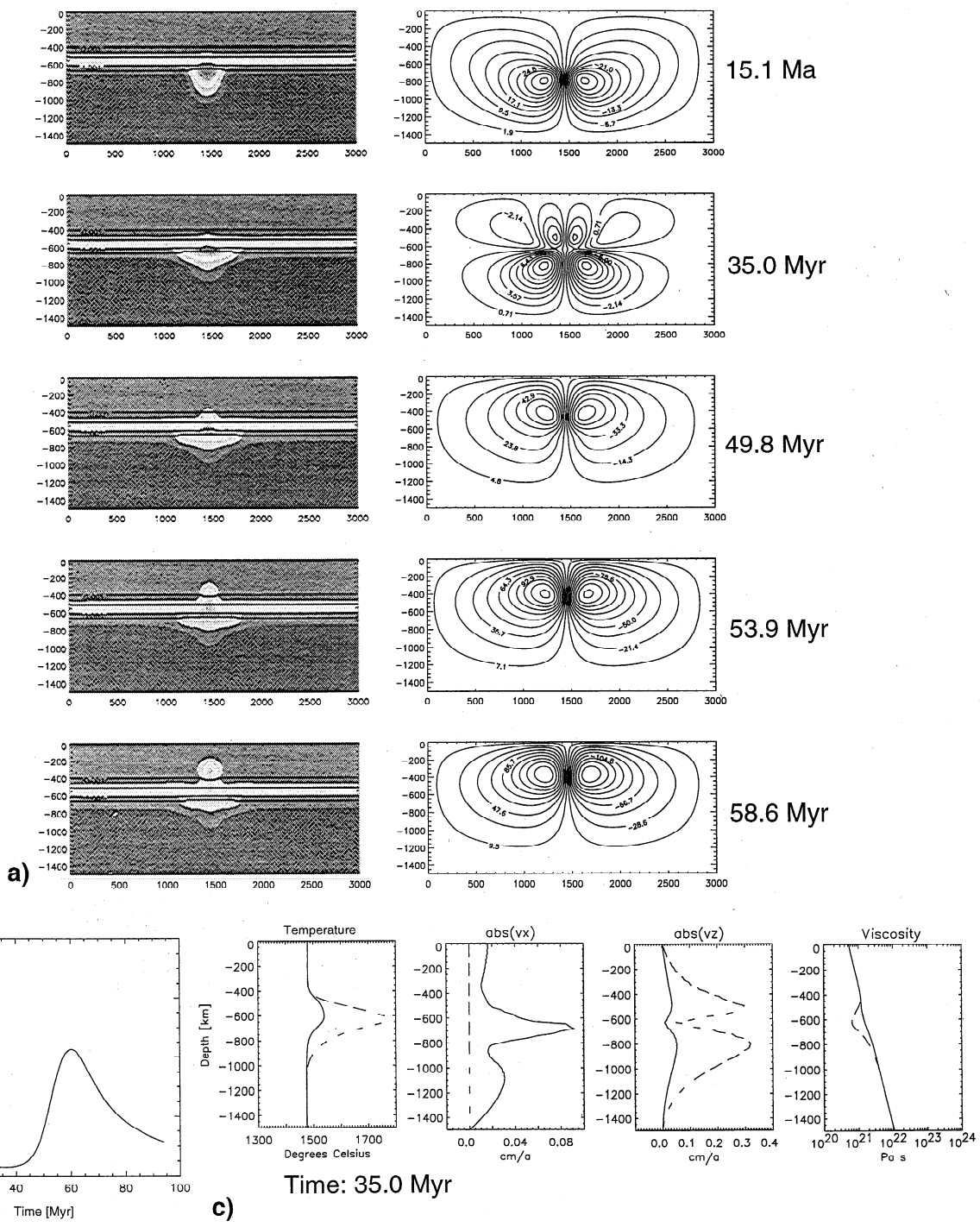

Figure 12. As in Figure 9, but for delayed penetration case using temperature and depth dependent viscosity and $P^* = 1.172$, $D = 0.311$. Notice the long interval of stagnating material at the phase transition. Stokes time based on the viscosity of the surrounding mantle at 600 km depth is 1.1 Myr.

rising from a thermal boundary layer and interacting with the S-P phase boundary. *Nakakuki et al.* [1994] modeled strong temperature-dependent viscosity and reported a clear dependence of penetration on the Rayleigh number. *Nakakuki et al.* [1994] interpret this dependence to reflect the influence of viscosity; however, our study suggests that viscosity is only indirectly the key. With increasing Rayleigh number the thickness of the thermal boundary layer decreases and so do the size of the rising plume heads evolving from this layer. The result of *Nakakuki et al.* [1994], therefore can be interpreted as the dependence of plume penetration on the size of the plume heads.

We have tested our parameterization on already published observations of the behavior of numerical plumes. Stagnating, partially penetrating, and penetrating plumes had been found for a 2-D Cartesian formulation by *Nakakuki et al.* [1994] and for a 2-D axisymmetric case by *Davies* [1995]. Plume radius and excess temperature were estimated from Figure 1 and 2 of *Nakakuki et al.* [1994] and from Figure 1 of *Davies* [1995] and by

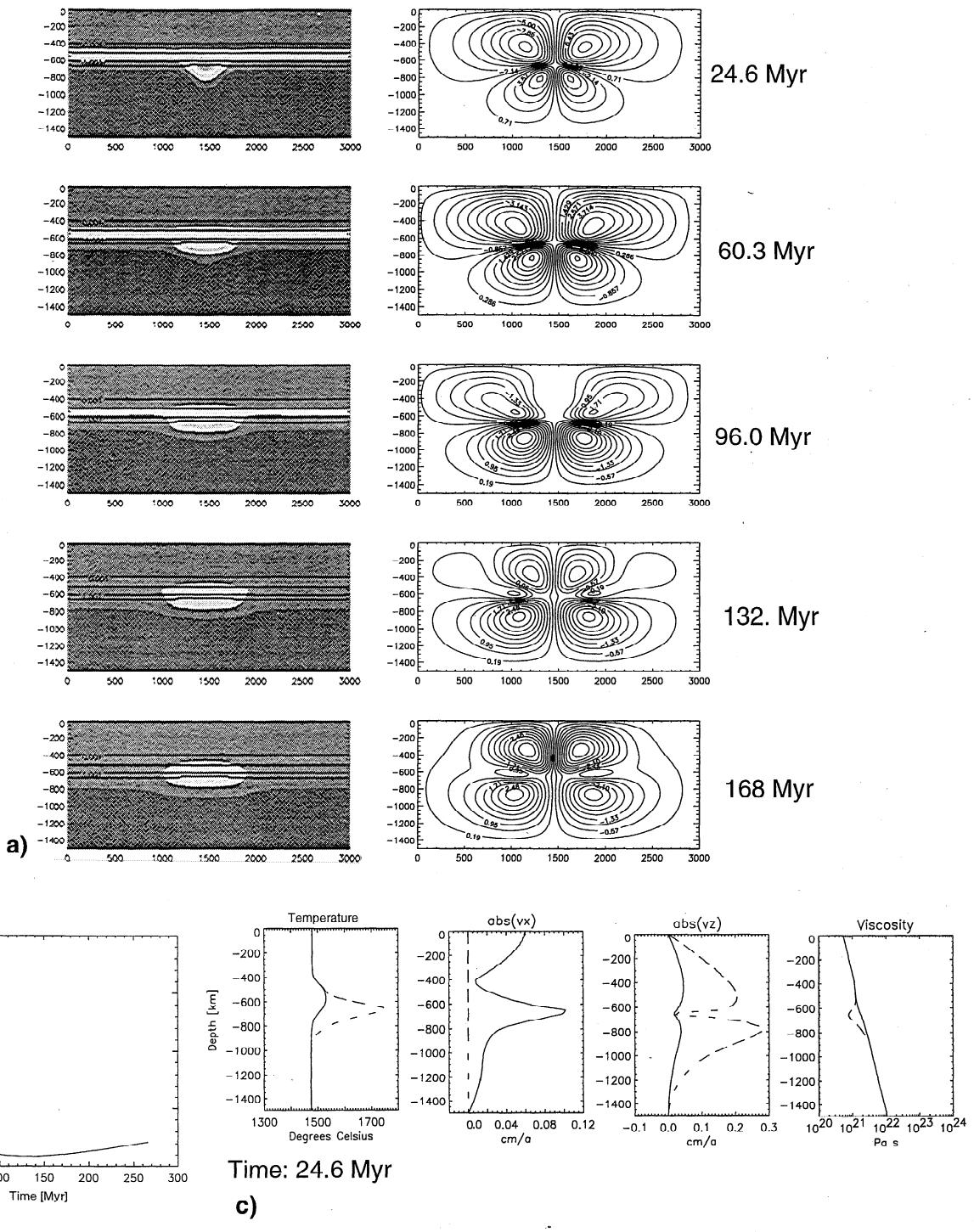

Figure 13. As in Figure 9, but for the stagnation case using temperature and depth dependent viscosity and $P^* = 2.28$, $D = 0.41$. Notice the layered convection with no penetration of plume material into the upper mantle. Stokes time based on the viscosity of the surrounding mantle at 600 km depth is 1.5 Myr.

personal communication with G. Davies (1999). Their results are marked by large symbols in Figure 8a and 8b. Even though there are broad uncertainties in estimating effective radii and excess temperatures, their numerical results fit quite well to our parameterization.

The effect of the plume conduit was neglected in our study. *Davies* [1995] observed in numerical models that while most of a plume head goes through the S-P phase boundary, the tail was blocked. It is difficult to use our results for studying the penetration of the plume conduit. In general, the influence of the plume conduit will depend on the relation between the diameter of the plume head and the plume conduit. This relation is still under discussion and depends on a number of parameters and especially on the rheological behavior. The results of the numerical modeling by *van Keken* [1997] show that the ratio between the radius of the plume head and the plume stem is ~3-4 for temperature-dependent viscosity for a wide range of Rayleigh numbers. The same ratio can also be obtained from laboratory

experiments by *Griffiths and Campbell* [1990]. For constant viscosity the ratio was considerably smaller, ~2.5 in the numerical experiments, but for stress-dependent rheology the plume conduits become very thin. Starting from the assumptions that the plume conduit even below the S-P phase boundary is considerably smaller than the head and that the thermal buoyancy created in the plume conduit is balanced locally by external and internal friction, so that a plume head will not be "pushed" by the conduit, we calculated some models with minor volumes following a larger one in a short distance. It turned out that if the first volume (plume head) is penetrating, it starts a flow and establishes a temperature field across the S-P phase boundary which facilitates the penetration of the following ones even if they lie in the stagnation regime. If the first volume is stagnating and spreading, the following minor volumes increase the amount of material but do not increase the ability to penetrate. Thus our findings on penetration and stagnation are not very sensitive to the existence of the conduit.

Application of our results to the Earth requires constraints on the size of plume heads. This topic has been addressed in a number of observational and theoretical studies. *Richards* [1989] suggested that many of the Earth's major flood basalt provinces formed by the rapid melting of plume heads, as they impinge upon the lithosphere. *Coffin and Eldholm* [1993] computed the volume of mantle material required to generate seven of the Earth's flood basalt provinces. Lower-bound estimates are calculated by assuming 30% partial melting and suggest spherical volumes with radii ranging from ~100 km for the Columbia River basalts to ~350 km for the Ontong Java Plateau. Upper-bounds estimates, assuming 5% partial melting, suggest radii of ~180 km-600 km for Columbia River and Ontong Java, respectively.

White and McKenzie [1989] speculated on very large thermal anomalies below the lithosphere preceding continental rifting events. On the basis of observations on related flood basalt provinces they claimed diameters of these anomalies >2000 km. Even though the plume head spreads below the lithosphere, this implies an effective radius for the spherical plume head of ~300 km (assuming a flattening of 0.1 of the plume below the lithosphere). Even larger plumes have been postulated by *Griffiths and Campbell* [1990], who studied entrainment in plumes using labroratory experiments with plume injection and compared their results to observations on extrusiva from flood basalt provinces. On the basis of the observation of large amounts of entrainment in their laboratory models, they claimed plume heads to have radii of ~500 km when reaching the upper mantle. However, entrainment in plumes is critically influenced if plumes result from a thermal boundary layer or if they are triggered by material injection [*van Keken*, 1997; U. Hansen, personal communication, 1998].

Numerical 2-D cylindrical experiments on the evolution of plumes from a thermal boundary layer by *van Keken* [1997] resulted in plumes with effective radii of the order of 120-170 km for Rayleigh numbers of $4.4\text{x}10^7$-$5\text{x}10^6$. He found that the size of the plume head is not very sensitive to the specified rheology. *Davies* [1995] found somewhat larger plume heads (with an effective radius of the order of 240 km) but obtained stagnating plumes by assuming more olivine in the mantle and a larger density jump across the S-P phase boundary. The size of a mantle plume simulated in laboratory and theoretical models depends on the conditions at the source layer, i.e. the thickness of the thermal boundary layer at the core mantle boundary which scales with the Rayleigh number in the way that large plumes arise under low Rayleigh number conditions. The largest uncertainty in these calculations is the effective viscosity of the mantle.

There seems to be agreement that flood basalt provinces are created by large plumes with effective radii of >200 km. But are there indications of the existence of smaller plumes in the Earth's mantle? The effects of large plumes are easy to observe since these anomalies have reached the upper mantle and passed the S-P phase boundary presumably without being much affected. Completely stagnated plumes would not lead to any surface volcanism, but partial (or delayed) penetrating plumes create small plumes with reduced excess temperature rising through the upper mantle. The existence of a large number of small seamounts on the ocean floors not connected to any hotspot tracks is evidence for localized volcanism. These seamounts are primary candidates for surface expressions of small plumes. However, the question is still not decided whether small plumes may possibly also originate at the base of the upper mantle. Even in this case, these plumes must be triggered by thermal fluctuations presumably arising from the lower mantle.

Partial (delayed) penetration and stagnation may also play an important role for the chemical composition of minor plumes feeding volcanic island chains. *Halliday et al.* [1995] investigated incompatible trace elements in a number of Atlantic seamounts and found that the magmas could not be derived from a MORB-like source but demand source regions that involve less depleted heterogeneous material, dispersed in the asthenosphere. It may be conjectured that such heterogeneities in minor plumes may strongly depend on the interaction between the plume and the S-P phase boundary, in particular for partially penetrating plumes. Our results suggest that incorporation of mantle material from the S-P phase boundary into plumes will be small for hot and large plumes and become more important for less hot and smaller plumes.

Appendix: P^* and D Values for Spheres and Cylinders of Different Flattening

Thermal buoyancy is created in the entire volume of a hot plume head V_0, but phase buoyancy is created only in that part of the volume V' where the phase transition curve is deflected. Thus the force ratio between phase and thermal buoyancy, F_{ph}/F_T, is given by

$$\frac{F_{ph}}{F_T} = \frac{\Delta\rho\ g\ V'}{\alpha\ \Delta T\ \rho_0\ g\ V_0}\ . \tag{A1}$$

We determine V_0 and V' for flattened spheres and cylinders and the related caps and internal sheets as indicated in Figure 2a and 2b. Considering the definitions for P^* and D (equations (4) and (5)), we derive the following expressions, where f is the flattening parameter:

for the case shown in Figure 2a and spheres,

$$P^* = \frac{4}{3}\ D\ (1-f)^{2/3} \left(D - \frac{1}{3\ (1-f)^{4/3}} \left[(1-f)^2 - \left((1-f)^{2/3} - D \right)^3 \right] \right)^{-1}; \tag{A2}$$

for the case shown in Figure 2b and spheres,

$$P^* = \frac{4}{3}\ (1-f)^{2/3} \left[1 - \frac{D^2}{12\ (1-f)^{4/3}} \right]^{-1}; \tag{A3}$$

for the case shown in Figure 2a and cylinders,

$$P^* = D\ \pi \left(\arccos\frac{(1-f)^{1/2} - D}{(1-f)^{1/2}} - \frac{(1-f)^{1/2} - D}{(1-f)^{1/2}} \left[1 - \frac{\left((1-f)^{1/2} - D \right)^2}{(1-f)} \right]^{1/2} \right)^{-1}; \tag{A4}$$

for the case shown in Figure 2b and cylinders,

$$P^* = D\ \pi \left(\pi - 2\ \arccos\frac{D}{2\ (1-f)^{1/2}} + \frac{D}{(1-f)^{1/2}} \left[1 - \frac{D^2}{4\ (1-f)} \right]^{1/2} \right)^{-1} \tag{A5}$$

Acknowledgments. This study was the result of a number of discussions during a research visit by two of the authors (G. Marquart and H. Schmeling) to the University of Hawaii at Manoa. Besides the valuable discussions this study also benefitted from the friendly atmosphere at the University of Hawaii and the impressive landscape. The paper gained a lot from reviews by G. Davies, U. Christensen, and an anonymous reviewer. This work was supported by the Deutsche Forschungs-gemeinschaft under the research grants Sch 876/6 and Ja 258/34 and a travel grant given to one of the authors (H. Schmeling).

References

Akaogi, M., E. Ito, and A. Navrotsky, Olivine-modified spinel-spinel transitions in the system Mg_2SiO_4 - Fe_2SiO_4: Calorimetric measurements, thermochemical calculation, and geophysical application, *J. Geophys. Res., 94,* 15,671 - 15,685, 1989.

Akaogi, M., H. Kojitani, K. Matsuzaka, T. Suzuki, and E. Ito, Postspinel transformations in the system Mg_2SiO_4 - Fe_2SiO_4: Element partitioning, calorimetry, and thermodynamics calculation, in *Properties of Earth and Planetary Materials at High Pressure and Temperature, Geophys. Monogr Ser., Vol. 101,* edited by H. H. Manghnani and T. Yagi, pp. 373 - 384, 1998.

Bercovici, D., G. Schubert, and P. J. Tackley, On the penetration of the 660 km phase change by mantle downflows, *Geophys. Res. Lett., 20,* 2599 - 2602, 1993.

Bijwaard, H., and W. Spakman, Tomographic evidence for a narrow whole mantle plume below Iceland, *Earth Planet. Sci. Lett., 166,* 121 - 126, 1999.

Chopelas, A., and R. Boehler, Thermal expansion measurements at very high pressure, systematics, and a case for a chemically homogeneous mantle, *Geophys. Res. Lett., 6,* 1347 - 1350, 1989.

Christensen, U. R., and D. A. Yuen, Layered convection induced by phase transitions, *J. Geophys. Res., 90,* 10,291 - 10,300, 1985.

Coffin, M. F., and O. Eldholm, Scratching the surface: Estimating dimensions of large igneous provinces, Geology, *21,* 515 - 518, 1993.

Davies, G. F., Penetration of plates and plumes through the mantle transition zone, *Earth Planet. Sci. Lett., 133,* 507 - 516, 1995.

Griffiths, R. W., and I. H. Campbell, Stirring and structure in mantle starting plumes. *Earth Planet. Sci. Lett., 99,* 66-78, 1990.

Halliday, A. N., D.-C. Lee, S. Tommasini, G. R. Davies, C. R. Paslick, J. G. Fitton, and D. E. James, Imcompatible trace elements in OIB and MORB and source enrichment in the sub-oceanic mantle, *Earth Planet. Sci. Lett., 133,* 379 - 395, 1995.

Honda, S., D. A. Yuen, S. Balachandar, and D. Reuteler, three-dimensional instabilities of mantle convection with multiple phase transitions, *Science, 259,* 1308 - 1311, 1993.

Ito, E., and E. Takahashi, Postspinel transformations in the system Mg_2SiO_4 - Fe_2SiO_4 and some geophysical implications, *J. Geophys. Res., 94,* 10,637 - 10,646, 1989.

Katsura, T., and E. Ito, The system Mg_2SiO_4 - Fe_2SiO_4 at high pressures and temperatures: Precise determination of stabilities of olivine, modified spinel, and spinel, *J. Geophys. Res., 94,* 15,663 - 15,670, 1989.

Machetel, P., and P. Weber, Intermittent layered convection in a model mantle with an endothermic phase change at 670 km, *Nature, 350,* 55 - 57, 1991.

McKenzie, D., and M. J. Bickle, The volume and composition of melt generated by extension of the lithosphere, *J. Petrol., 29,* 625 - 679, 1988.

Morgan, W. J., Convection plumes in the lower mantle, *Nature, 230,* 42 - 43, 1971.

Nakakuki, T., H. Sato, and H. Fujimoto, Interaction of the upwelling plume with the phase and chemical boundary at the 670 km discontinuity: Effects of temperature-dependent viscosity, *Earth Planet. Sci. Lett., 121,* 369 - 384, 1994.

Peltier, W. R. and L. P. Solheim, Mantle phase transitions and layered chaotic convection, *Geophys. Res. Lett., 19,* 321 - 324, 1992.

Richards, M. A., R. A. Duncan and V. E. Courtillot, Flood basalts and hot-spot tracks: Plume heads and tails. *Science, 246,* 103 - 107, 1989.

Schubert, G., and D. L. Turcotte, Phase transitions and mantle convection, *J. Geophys. Res., 76,* 1424 - 1432, 1971.

Schubert, G., D. A. Yuen, and D. L. Turcotte, Role of phase transitions in a dynamic mantle, *Geophys. J. R. Astron. Soc., 42,* 705 - 735, 1975.

Schubert, G., C. Anderson, and P. Goldman, Mantle plume interaction with an endothermic phase change, *J. Geophys. Res., 100,* 8245 - 8256, 1995.

Tackley, P. J.,On the penetration of an endothermic phase transition by upwellings and downwellings. *J. Geophys. Res., 100,* 15,477 - 15,488, 1995.

Tackley, P. J., D. J. Stevenson, G. A. Glatzmaier, and G. Schubert. Effects of multiple phase transitions in a three-dimensional spherical model of convection in the Earth's mantle. *J. Geophys. Res., 99,* 15,877 - 15,901, 1994.

VanDecar, J. C., D. E. James, and M. Assumpcao, Seismic evidence for a fossile mantle plume beneath South America and implications for plate driving forces, *Nature, 378,* 25 - 31, 1995.

van Keken, P. E., and C. W. Gable, The interaction of a plume with a rheological boundary: A comparison between two- and three-dimensional models, *J. Geophys. Res., 100,* 20,291 - 20,302, 1995.

van Keken, P., Evolution of starting mantle plumes: a comparison between numerical and laboratory models, *Earth Planet. Sci. Lett., 148,* 1 - 11, 1997.

White, R., and D. McKenzie, Magmatism at rift zones: The generation of volcanic continental margins and flood basalts, *J. Geophys. Res., 94,* 7685 - 7729, 1989.

Wolfe, C. J, I. T. Bjarnarson, J. C. VanDecar, and S. C. Solomon, Seismic structure of the Iceland mantle plume, *Nature, 385,* 245 - 247, 1997.

Zhao, W., D. A. Yuen, and S. Honda, Multiple phase transitions and the style of mantle convection, *Phys. Earth Planet. Inter., 72,* 185 - 210, 1992.

G. Ito, School of Ocean and Earth Science and Technology, University of Hawaii at Manoa, 2525 Correa Road, Honolulu, HI 96822. (gito@soest.hawaii.edu)

G. Marquart and H. Schmeling, Institute of Meteorology and Geophysics, J. W. Goethe University Frankfurt, Feldbergstraße 47, D-60323 Frankfurt, Germany. (marquart@geophysik.uni-frankfurt.de; schmeling@geophysik.uni-frankfurt.de)

B. Schott, Department of Geoscience, Uppsala University, Villavägen, S-75236 Uppsala, Sweden. (bs@geofys.uu.se)

(Received April 21, 1999; revised September 30, 1999;
accepted November 15, 1999.)